Proceedings of
11th European Conference on Turbomachinery Fluid dynamics & Thermodynamics
ETC11, March 23-27, 2015, Madrid, Spain

EXPERIMENTAL INVESTIGATIONS OF SECONDARY FLOW DEVELOPMENT AROUND TANDEM VANES IN A 2D LINEAR STATOR COMPRESSOR CASCADE

A. Heinrich - C. Tiedemann* - D. Peitsch**

*Department of Aeronautics and Astronautics
Technische Universität Berlin
Berlin, Germany
E-Mail: alexander.heinrich@ilr.tu-berlin.de

ABSTRACT

Wake flow measurements and multi-colored oil flow visualizations were performed in a 2D linear stator compressor cascade for tandem configurations. Two sets of tandem vanes with different load split (LS) are compared to a set of conventional single vane reference blades. The measurements were performed at a Mach number of 0.6 and a Reynolds number of 900.000. During the experiments the tangential displacement (percent pitch PP) is varied from 85% to 95% for the tandem blade configurations. The results of the oil flow visualization in addition with wake flow measurements show how the secondary flow structures develop and change with varying tangential displacement.

NOMENCLATURE

Symbols

c	m	chord length
c_{xy}	m/s	in-plane velocity magnitude
δ_{99}	m	boundary layer thickness
i	°	incidence
κ	°	flow angles
Ma	1	Mach number
Re	1	Reynolds number
s	m	distance TE (AB) - LE (FB)
t	m	blade pitch
x, y, z	m	coordinate system
ω	1	total pressure loss coefficient

Abbreviations

AB	aft-blade
AO	axial overlap
CDA	Controlled Diffusion Airfoil
DF	diffusion factor
DH	deHaller factor
FB	front-blade
FSO	full scale output
LE	leading edge
LS	load split
PP	percent pitch
PS	pressure side
SS	suction side
TE	trailing edge
TUB	Technische Universität Berlin

INTRODUCTION

Modern tandem compressor research primarily focuses on the evaluation of geometric and aerodynamic optimum parameters for an effective and preferably low-loss turning and pressure rise. Primary areas of focus are the load distribution LS between the two blades, the choice of diffusion factor DF and axial as well as tangential offset (so-called *axial overlap* AO and *percent pitch* PP) of the blades (cf. Fig. 2).

One of the most recent investigations were carried out by McGlumphy (2008). He focused his research on the detailed numeric simulation of a rotor tandem configuration for the last stages of an

axial compressor. His suggestions for a load split share of $LS = 50/50$ found their way into this work. In addition, the work by Schluer et al. (2009) and Falla (2004) was also used during the design phase. The experimental investigations by Trehan and Roy (2007), Trehan et al. (2008) as well as Sturm (1988) helped to set the scope for the experimental work. Trehan et al. concentrated on the detailed investigation of the gap flow between the front- and aft-blade. Sturm analyzed the usage of slots in the profile geometry for controlling the boundary layer development and in particular the influence of the geometry of the slot at the flow separation control. Frey and Böhle (2013) very recently also examined the influence of the percent pitch variation for a 50% load split tandem configuration. They proved that tandem cascades with a percent pitch of $PP = 90\%$ achieve lower pressure losses compared with those with a percent pitch of 70%.

In summary, tandem configurations have proven to have a great potential in terms of reduced overall losses and flow turning in contrast to conventional blade designs during previous 2D-evaluations. Thus they are appropriate for a specific turning- and load distribution and different Mach number ranges. The load distribution between the front- and the aft-blade has a strong impact on the secondary flow development on the particular blade. According to current state of research, it is also evident that the evaluation of three-dimensional flow phenomena is rather difficult at this stage. Moreover, the extreme influence of the present secondary flow phenomena has not been acknowledged in a sufficient manner. As a consequence there is a high demand for research in order to evaluate the characteristics of different geometric configurations in combination with the present flow conditions with regard to an optimization of the aforementioned topics.

In the following chapters, an overview of the linear compressor stator test rig is given in chapter *EXPERIMENTAL FACILITY*. The experimental setup as well as the measurement techniques used are briefly described in *EXPERIMENTAL SETUP AND PROCEDURES*. The corresponding experimental findings are presented in chapter *RESULTS*. At first, the flow phenomena around the single reference blade are analyzed (see section *Base configuration*) followed by the detailed investigation for the two tandem configurations at the design percent pitch of $PP = 91\%$. Subsequently, a variation of the percent pitch of 85% and 95% is experimentally investigated and compared to the results.

EXPERIMENTAL FACILITY

The high-speed wind tunnel and the compressor cascade used for these investigations have been designed at the Chair of Aero Engines at *TUB* and is shown in Figure . The design is that of an open wind tunnel, the so-called *Eiffel* design. The wind gallery consists of a diffuser, settling chamber, a nozzle and the compressor cascade itself. Different screens and flow conditioners inserted in the diffuser and inside the settling chamber rectify the flow before it enters the nozzle to provide uniform conditions at the cascade inlet.

The wind tunnel system is fed by three radial compressors with a combined output of $1\,MW$. All three compressors can be independently controlled, allowing different mass flows and pressure ratios. Each compressor has a pressure ratio of $\Pi = 2$ and a massflow of $\dot{m}_{air} = 1.5\,kg/s$. Different connection settings allow the provisioning of different inflow conditions for the test section. The test section has a cross-sectional area of $63 \times 256\,mm$. For blades placed in the cross-section, Mach numbers from $Ma = 0.3 - 0.9$ for corresponding Reynolds numbers between $0.45 \times 10^6 - 1.3 \times 10^6$ (based on axial chord length) can be established. In addition, an intercooler can also be added which allows to vary the Reynolds number by constant Mach number.

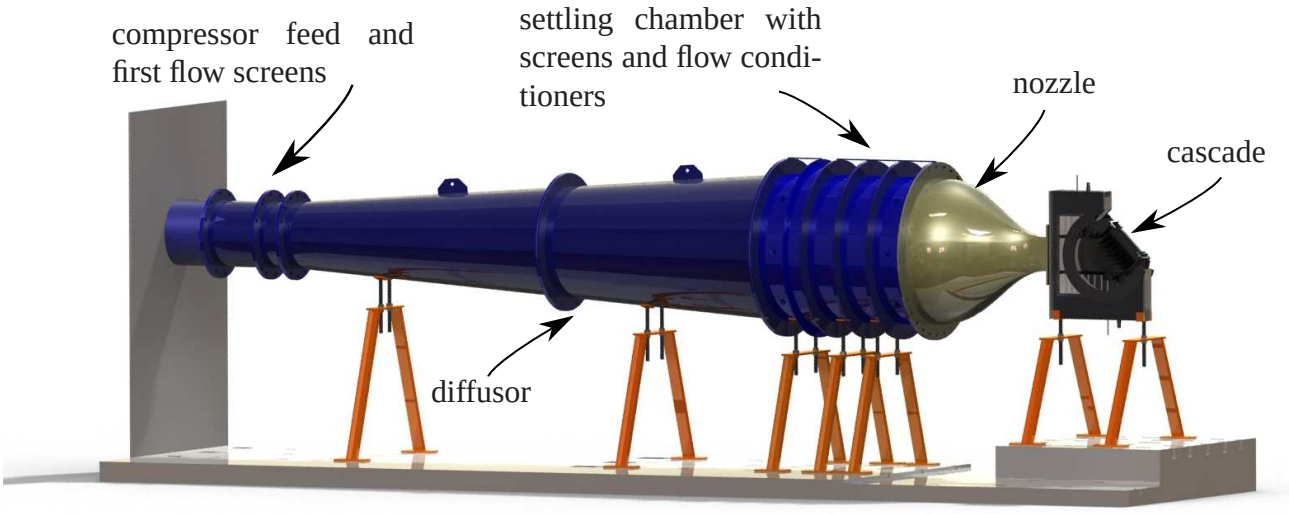

Figure 1: **wind tunnel gallery**

Geometry of the Cascade

The profile of the blades used for these experiments have been designed by *Rolls-Royce Deutschland Ltd. & Co.KG* and is similar to blades used in current engine applications in terms of size and shape. The aerodynamic design is based on a purely two dimensional evaluation of the flow field (sectional design) with the starting for the design approach being based on the work by McGlumphy and NG (2007). The tandem vane geometry development was carried out using *MISES* and the *Rolls-Royce Deutschland Ltd. & Co.KG* tool *HYDRA* (3D-CFD, full turbulent, SA-Tu model, grid generation with Numeca Autogrid) for the section.

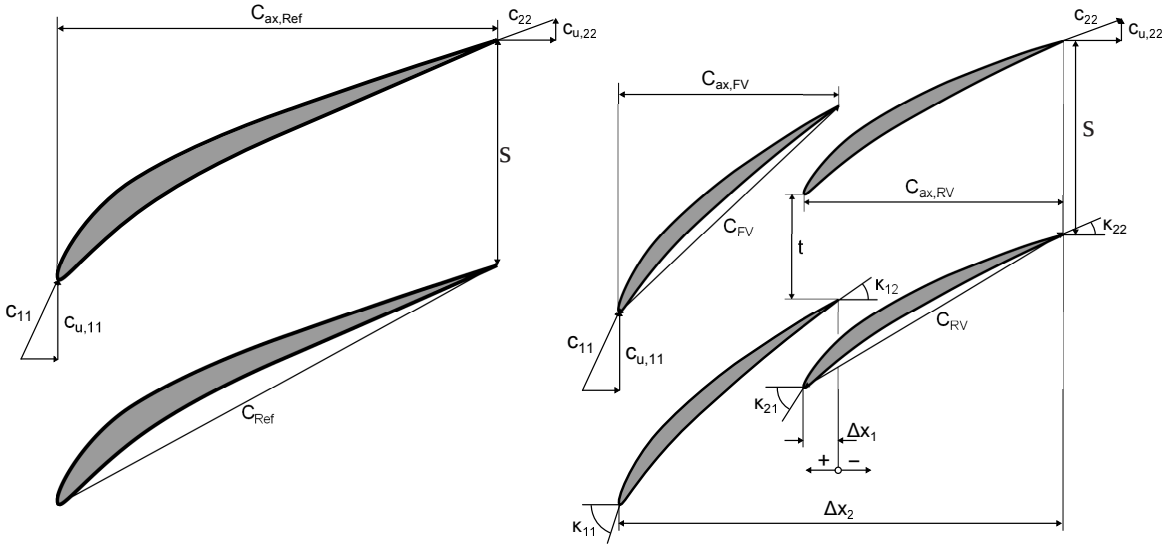

single blades tandem blades

Figure 2: **Tandem Blade Geometrical Parameters**

The blades are designed as controlled diffusion airfoils (CDA) with a highly loaded aerodynamic profile. The single reference blades have a chord length of $c = 63\,mm$ with a blade aspect ratio of $s/c = 1.0$ and a pitch-to-chord ratio of $t/c = 0.5$. Both the design deflection angle and stagger angle are fixed to $\beta = 50\,^\circ$ and $\gamma = 20\,^\circ$ respectively. The cascade is designed to be operated at a Mach

Number of $Ma = 0.6$ and a chord based Reynolds Number of $Re = 0.9 \times 10^6$.An incidence variation of $\pm 10\,^\circ$ can be realized by rotating the moveable side wall.

The nomenclature for tandem vanes differs from ordinary single vanes and is shown in figure 2. Here, FB stands for the front-blades and AB for the aft-blades, respectively.
Two important geometric parameters when describing tandem blades are the axial overlap and the percent pitch. The axial overlap AO is described as

$$AO = \Delta\, x_1 / \Delta\, x_2 \tag{1}$$

The percent pitch PP is described as the tangential displacement of the two blades. The gap between the two blades increases the smaller the values are for the PP. It is defined as

$$PP = t/s \tag{2}$$

The load split LS is a parameter defining the work share between the front- and aft-blades. According to McGlumphy et al. (2009) a load split of $LS = 0.5$ is desirable when designing tandem vanes. In the course of the experiments two sets of tandem vanes with different load splits are analyzed. The following two equations (cf. Eqn. 3 and 4) describe the definitions used for the Load Split. The first one uses the diffusion factor DF and the second the *deHaller* coefficient DH.

$$LS_{DF} = \frac{DF_1}{DF_1 + DF_2} \tag{3}$$

$$LS_{DH} = \frac{DH_1}{DH_1 + DH_2} \tag{4}$$

The adjustment of the load split (LS) was done in the design program defining the upstream and downstream flow angle. As can be seen from the values in Table 1, the flow angles are similar to those of an outlet guide vane application. The tandem vanes have a chord length of $c_1 = c_2 = 31.5\,mm$ and the same maximum thickness for both front and rear vane of $t/c_1 = t/c_2 = 0.1$. The single reference blade and both tandem configurations show a similar thickness / camber-line-angle distribution along the relative chord length. The design percent pitch (PP) is set to $PP = 91\,\%$ and the axial overlap (AO) to $AO = 0.5$. Both the reference and the tandem vanes are designed to realize a working range of $5°$. As tandem blades can withstand a higher blade loading before flow separation occurs, the blade pitch is subsequently varied in order to meet the aforementioned design criterion.

The main geometric design parameters of the tandem vanes are summarized in Table 1.

case	Tandem	$\kappa_{11}\,[^\circ]$	$\kappa_{12}\,[^\circ]$	$\kappa_{21}\,[^\circ]$	$\kappa_{22}\,[^\circ]$	$\Delta\,[^\circ]$	s/c	LS_{DH}	LS_{DF}
#1	FB	50.00	37.62	-	-	12.38	0.51	0.50	0.42
#1	AB	-	-	37.62	0.00	37.62	0.51	0.50	0.42
#2	FB	50.00	33.45	-	-	16.55	0.45	0.47	0.50
#2	AB	-	-	33.45	0.00	33.45	0.45	0.47	0.50

Table 1: tandem geometric parameters

In addition to previous experiment (cf. Heinrich et al. (2014)), a percent pitch variation has been added to the cascade to allow for the examination of this influence on the secondary flow development

especially on the rear blade in future experiments. A variation of the axial overlap is only analyzed numerically and not part of the experimental investigations and therefore not subject of this paper.

Also, the incoming boundary layer can be increased by inserting extension segments to the wind tunnel. This is of particular interest as it is believed to also strongly influence the secondary flow development around the tandem blades.

EXPERIMENTAL SETUP AND PROCEDURES

An experimental investigation was carried out on the 2D linear compressor stator cascade of the Department of Aeronautics and Astronautics at the Berlin Institute of Technology. This test rig has already been used in other publications for Active Flow Control investigations such as Tiedemann et al. (2012a) and Tiedemann et al. (2012b). To investigate the flow phenomena on the compressor stator cascade, different measurement techniques were used.

Test rig and Test conditions

The experiments shown here were carried out at a Mach number of $Ma = 0.6$ and a corresponding Reynolds number of $Re = 900.000$ (based on axial chord length). The total temperature was set to $T_t = 50\,°C$ using the intercooler. The turbulence intensity is $< 1\%$ and the boundary layer thickness $\delta_{99} = 6\%c$.

Wakeflow measurements

To quantify the losses produced by these secondary flow phenomena wake measurements were conducted. A five-hole probe was used for the measurement of the downstream characteristics of the cascade. By means of this probe the magnitude of all three velocity components V_x, V_y and V_z of a flow vector, the static pressure p, the total pressure p_t as well as the spatial flow angle can be determined. The straight probe features a head diameter of $1.6\,mm$ and was installed at a three-axis traversing system allowing two-dimensional wake measurements at different positions. Figure 3 schematically shows the experimental setup for the wake measurements. The measurement plane is located half the chord length downstream of the trailing edge. The spanwise resolution is limited by a $3\,mm$ offset to the sidewall due to the size of the five-hole-probe (cf. Fig 3).

According to Liesner et al. a loss definition is realized in order to evaluate the loss production of each configuration Liesner and Meyer (2008).

The total pressure loss coefficient is defined as

$$\omega = \frac{p_{t1} - p_{t2}}{p_{t1} - p_1} \tag{5}$$

with Index 1 representing the inflow and 2 the measurement plane respectively. The total pressure of the inflow p_{t1} is measured with a pitot tube in the settling chamber which is connected to a differential pressure sensor (Sensortechniques HDO series) with a pressure range of $0 - 1$ bar and an uncertainty of max. $\pm 0.5\%$ Full Scale Output (FSO). The static pressure of the inflow is measured half a chord length upstream of the blades using the same pressure sensors. The measurement ports of the five-hole-probe are connected via flexible pressure tubes with differential pressure sensors (Sensortechniques HDO series) with a pressure range of 0 - 2 bar and an uncertainty of max. $\pm 0.5\%$ Full Scale Output (FSO). The deviation of the loss coefficient produced by error propagation amounts to $\pm 1.54\%$ corresponding to the mean loss of the design case.

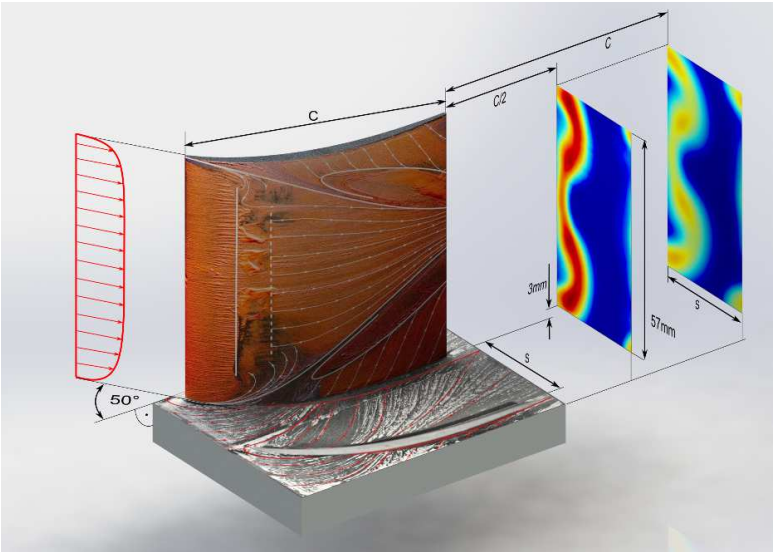

Figure 3: Measurement Planes

Oil flow visualization

The flow phenomena on the blade surface are visualized using the oil flow pattern method. The oil mixture is composed of thick liquid paraffin oil with blue, green, and red fluorescent pigments with an average grain size of $5\,\mu m$. The oil mixture for the sidewalls was composed using the same liquid paraffin oil but was mixed with white pigments of titanium dioxide which through its nano structure allows a higher resolution. The mixtures were painted onto the blade surface and the sidewalls and dried in the course of the experiment. The particles follow the surface streamlines in the boundary layer. The particle motion depends on the balance between the pressure gradient from outside the boundary layer and the shear stresses in the boundary layer. Where the skin friction approaches zero the color is completely removed by the flow, so separation lines are visible as black lines (cf. Maltby (1962)). After the drying process the blade's pressure and suction sides are photographed perpendicular to the chord using a high-resolution digital camera.

RESULTS

Base configuration

In order to rate the performance of the two tandem configurations against a single reference blade it is necessary to characterize the flow phenomena around this blade. Figure 4 shows the oil flow pattern for the reference blade at 0° incidence and a Mach number of $Ma = 0.60$. Depicted on the left hand side is a view of the suction side. The flow direction is from left to right, the leading edge of the blade is positioned at 0% c at the x-axis while the trailing edge lies at 100% c. The zero position of the y-axis is located at midspan. At about 20% c a separation bubble occurs followed by an attachment line at around 30% c. A strong corner vortex starts to develop at about 25% c on both sides. Adjacent to the corner vortex a large area of backflow region can be seen reaching from 50% c until the trailing edge. This backflow region takes up to 35% span on each side, constricting the undisturbed flow in the midspan area to 20 - 30%. The passage vortex which transports fluid from the opposite pressure side to the suction side arrives at about 50% chord length (highlighted by the blue color). Also visible is the location where the pressure side leg of the horseshoe vortex of the opposite pressure side (white color) hits the suction side at about 45% c.

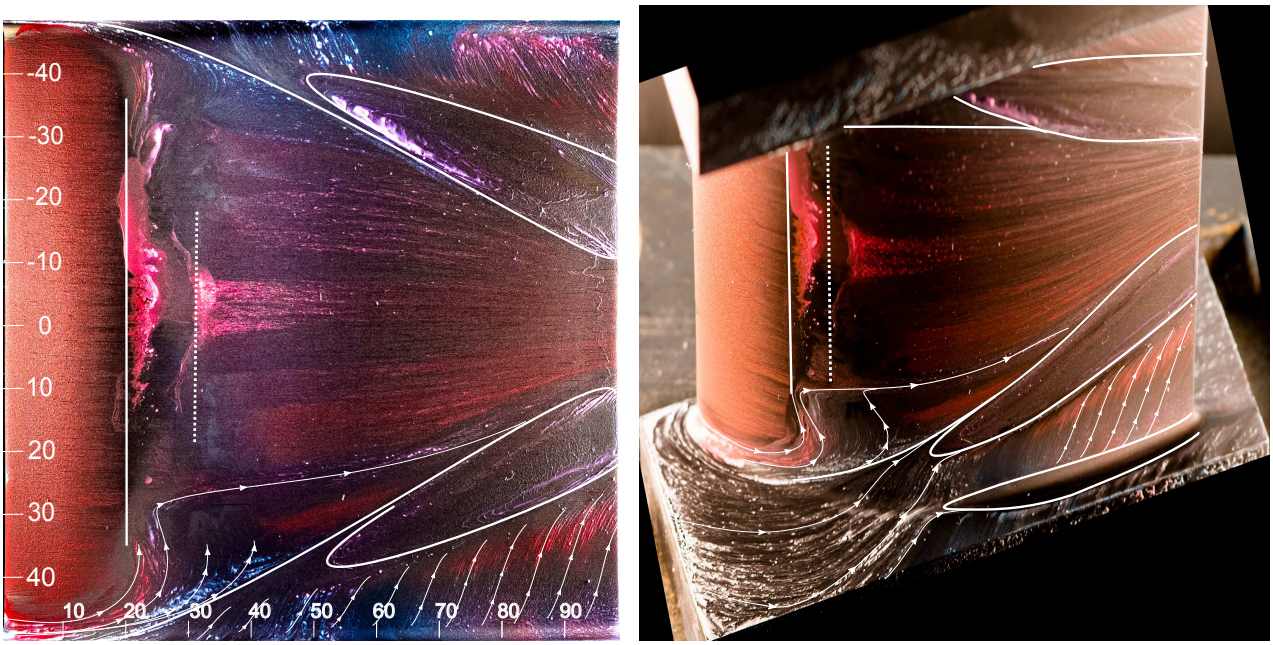

Figure 4: **Oil flow visualization for reference blade** $50°$ **turning angle,** $0°$ **incidence at** $Ma = 0.60$**. Depicted on the left hand side is a view of the suction side. (Color usage as follows: red color (suction side), blue color (pressure side) and white color (sidewall).)**

Tandem configuration with 91% **Percent Pitch (design point)**

Figure 5 shows the oil flow visualizations of the suction sides for the two tandem configurations at the design Percent Pitch of $PP = 91\%$. The pressure sides which are not presented here show a laminar flow distribution. The left two pictures show the suction side of the front-blade (FB) and the aft-blade (AB) for the $LS_{DH} = 0.5$ configuration. The general flow formation of the front blade is similar to that of the first half of the reference blade. A separation bubble is clearly visible again with a separation being positioned roughly around 25% c (please note: c is now the addition of the FB and AB chord) and the attachment line around 35% c. The development of the corner vortex starts at about 30% c and covers about 10% of the blade height on each side. There is a little bit of blue color visible on the trailing edge of the front blade. As the pressure sides were painted in blue, it could be concluded that fluid coming through the gap between the two blades has been drawn into a backflow region. However, it is too early to conclude this behavior at this stage. The flow pattern on the rear blade starts with an attachment line at about 55% total chord length. This is clearly visible by the green color representing the suction side flow from the front blade which has been lifted off the surface by the gap flow from the suction side of the FB.

It seems as if the impact point of both the pressure side leg of the horseshoe vortex from the opposite pressure side and the passage vortex are slightly shifted to the trailing edge of the rear blade. However the blue particles originate from the pressure side of the FB. The PS-leg of the horseshoe vortex and the passage vortex are blocked away from the suction side of the AB by the gap flow. This is clearly visible in Figure 6 and highlighted by the stream lines.

The right two pictures show the suction side of the front blade and the rear blade for the $LS_{DF} = 0.5$ tandem configuration. The overall layout is similar to that of the $LS_{DH} = 0.5$ configuration although there a few differences.

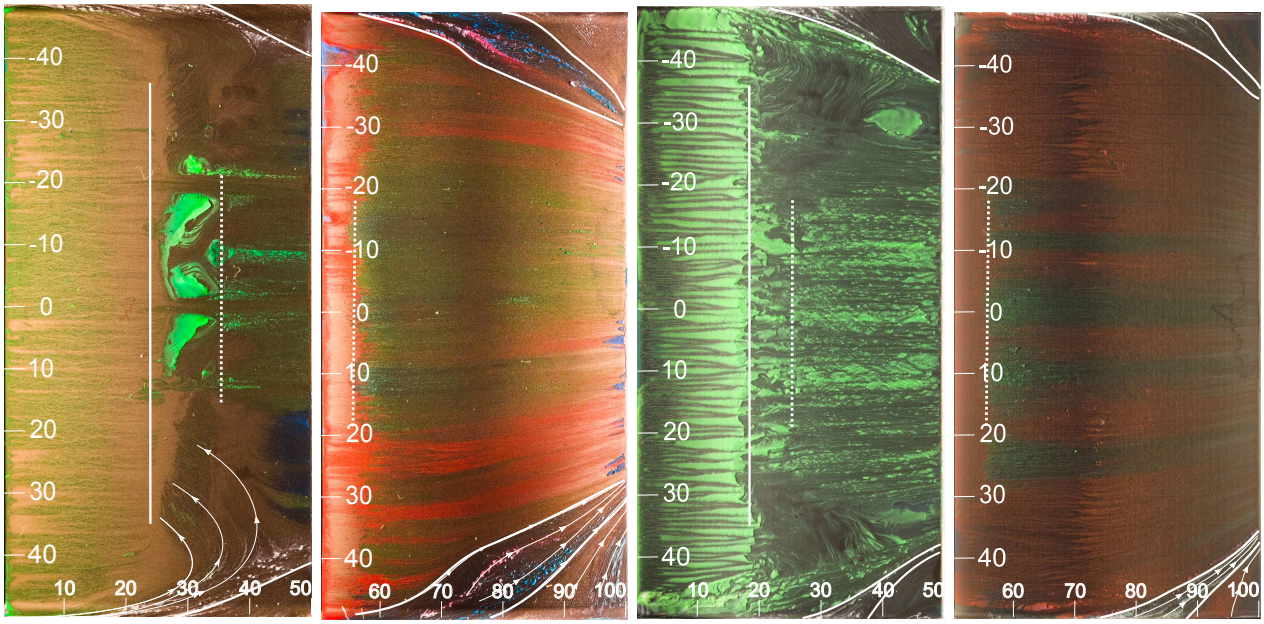

Figure 5: **Oil flow visualization of the suction side for tandem blades with $50°$ turning angle, $PP = 91\%$ (design point) at $0°$ incidence at $Ma = 0.60$. Depicted on the left hand side is the tandem configuration with $LS_{DH} = 0.5$ and $LS_{DF} = 0.5$ on the right hand side respectively. (Color usage as follows: green color (suction side FB), red color (suction side AB), blue color (pressure side of both FB and AB) and white color (sidewall).)**

The location of the separation bubble on the FB has moved by 5% to the leading edge. The reason for this is the increased blade loading as a result of the higher turning of the FB compared to case # 1 (cf. Table 1). The development of the corner vortex of the FB seems to be unaffected by the higher turning and shows the same dimension for case # 2. In contrast to the case #1 AB, the case #2 AB does not show any sign of blue paint. Furthermore it is noticeable that less green paint is visible on the AB and that the dimensions of the corner structures are well reduced. This is an indication for an increased strength of the gap flow which reduces the momentum exchange of the FB suction side's flow with that of the AB and also blocks off the passage vortex from hitting the AB (no blue particles visible).

Figure 6: **Close-Up of the oil flow visualization of the trailing edge and passage flow for the $LS_{DH} = 0.5$ tandem blade configuration with $50°$ turning angle, $PP = 91\%$ (design point) at $0°$ incidence at $Ma = 0.60$.**

Tandem configuration with 85% Percent Pitch

Figure 7 shows the oil flow visualization for a percent pitch variation of $PP = 85\%$. In this setup, the gap between the FB and AB has its maximum value positioning both the FB and AB furthest apart from each other.

The left two pictures characterize the flow for the $LS_{DH} = 0.5$ configuration. In contrast to Figure 5 one can easily notice the similar flow topology on both blades. The front blade shows a separation

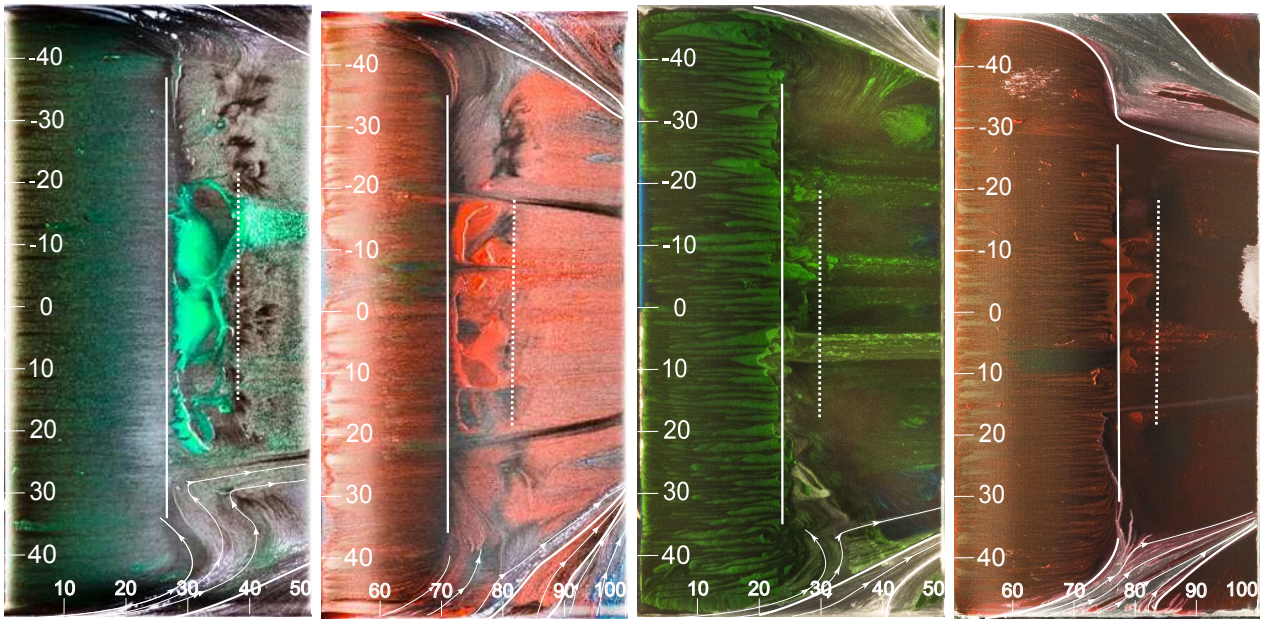

Figure 7: **Oil flow visualization of the suction side for tandem blades** $50°$ **turning angle,** $PP = 85\%$ **at** $0°$ **incidence at** $Ma = 0.60$**. Depicted on the left hand side is the tandem configuration with** $LS_{DH} = 0.5$ **and** $LS_{DF} = 0.5$ **on the right hand side respectively. (Color usage as follows: green color (suction side FB), red color (suction side AB), blue color (pressure side of both FB and AB) and white color (sidewall).)**

bubble at around 27% c followed by an attachment line at 37% c. The corner vortices start to develop around 30% c. The AB also features a separation bubble (starting at 70% c with an attachment line at 83%c) which is slightly positioned more upstream (compared relatively to the FB). Disregarding from a few minor green spots just before the separation line, no green color is evident on the AB suction side. The corner vortex structures are a bit more complex. Blue paint indicates that fluid from the opposite pressure side reaches the trailing edge of the AB and its spanwise dimension reaches up to 25% on each side constricting the main flow to the midspan area.

The $LS_{DF} = 0.5$ tandem configuration also shows an almost similar pattern on both FB and AB but in addition continues the same tendency as seen in Figure 5 before. The separation bubble on the FB occurs a little earlier than for the case #1 and the topology on the AB is more calm compared to the case #1 AB (missing of blue paint), although it still features a separation bubble (positioned from 75% c - 85% c). Again, the absence of green paint indicates that due to the increased gap size between FB and AB, the flow around the two blades can rather be considered as two separate flows.

Tandem configuration with 95% **Percent Pitch**

The oil flow visualizations in Figure 8 represent the results for the $PP = 95\%$ variation. In this setup, the front and rear blade have its closest tangential position to each other.

The flow structure on the front blade of the $LS_{DH} = 0.5$ configuration (left two pictures) is similar to the previous front blades of the same configuration. Clearly visible is the separation bubble with a width of around 13% c ranging from 22% - 35% chord length. The corner vortices develop around 30% c and take up to 10% in spanwise direction on both sides. The rear blade shows, for the first time, a 3D separation for a larger area in the midspan at the trailing edge and a strong development of the corner vortices (starting at 75% c and covering almost 25% in spanwise direction). The blue

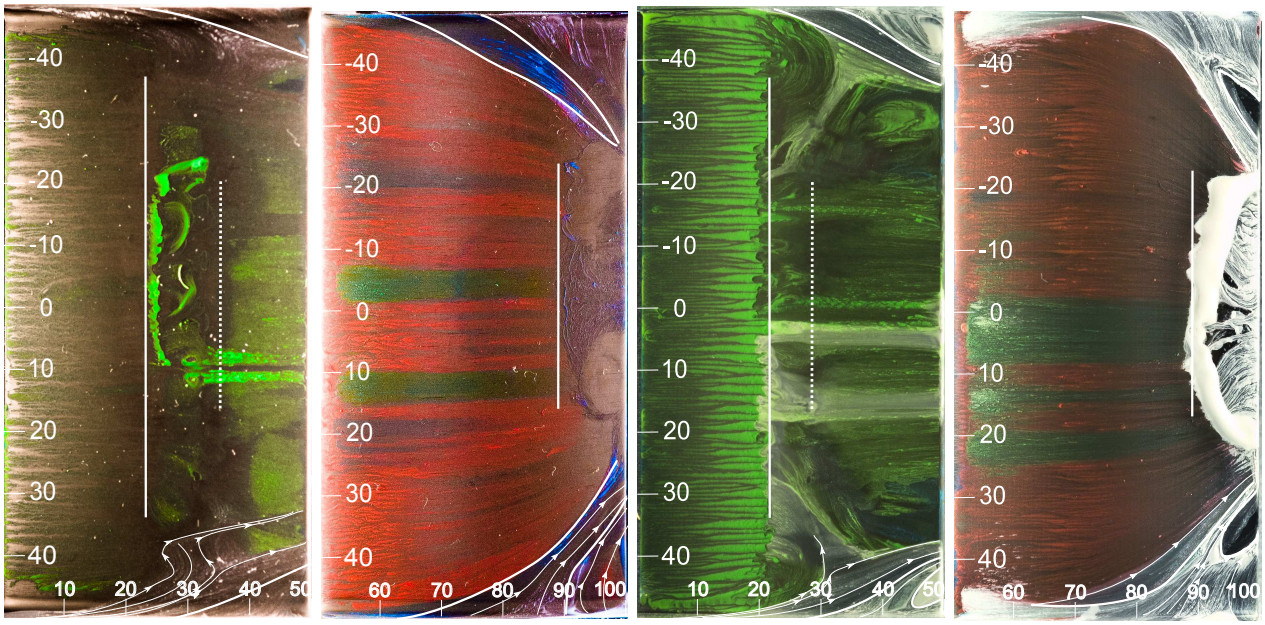

Figure 8: **Oil flow visualization of the suction side for tandem blades** $50°$ **turning angle,** $PP = 95\%$ **at** $0°$ **incidence at** $Ma = 0.60$**. Depicted on the left hand side is the tandem configuration with** $LS_{DH} = 0.5$ **and** $LS_{DF} = 0.5$ **on the right hand side respectively. (Color usage as follows: green color (suction side FB), red color (suction side AB), blue color (pressure side of both FB and AB) and white color (sidewall).)**

particles indicate that fluid from the FB pressure side coming through the gap is pushed onto the suction side. The small size of the gap between the FB and AB limits the development of a strong gap flow which is strong enough to encounter the passage cross flow and also would be able to prohibit the 3D separation at the AB TE.

The two pictures on the right hand side visualize to flow phenomena for the $LS_{DF} = 0.5$ tandem configuration. The front blade looks pretty similar to those previous case # 2 FB oil visualizations with a laminar turbulent transition point at around 21% c and a corner vortex development starting roughly at 25% c. For the first time visible is a little recirculation area at the TE of the FB starting at around 45%. The rear blade now is in good alignment with the case # 1 rear blade except for the missing blue particles. (The excessive amount of white particles at the TE are due to the shortened drying process.) The dimensions of the corner vortices are the same except for the fact that there is again a recirculation area starting at 93%.

Wake flow measurements

Figure 9 shows a selection of the conducted wake flow measurements for $0°$ incidence at $Ma = 0.60$ and a $PP = 91\%$ (for the tandem blades). These measurements represent the best case scenario for the minimum losses. Figure 9 a) shows the integral spanwise total pressure loss distribution for the single reference blade and both tandem configurations. Apart from the symmetry of the plots which is a sign for the good quality of the measurements, the different pressure loss characteristics are clearly visible.

Both tandem configurations (red lines) show a well reduced total pressure loss in the midspan area. In the sidewall area however, the trend is reversed and the single reference blade shows lower absolute values especially very close to the sidewall. These results are in good alignment with the oil

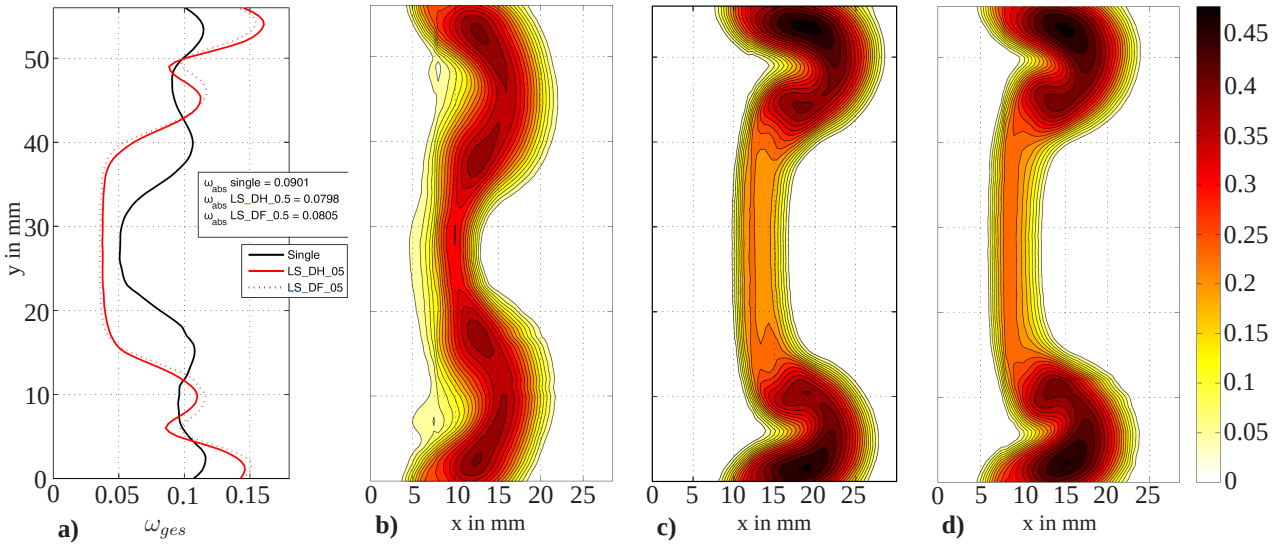

Figure 9: **Wake flow measurements at $Ma = 0.60$, $0°$ incidence and $0.5c$ behind trailing edge. a) Comparison of integral spanwise total pressure loss distribution ω_{ges}. b-d) Area plots of total pressure loss distribution for single reference blade (b), $LS_{DH} = 0.5$ (c) and $LS_{DF} = 0.5$ (d).**

flow visualizations in Figures 4 and 5 respectively. The visual conclusions that the expansion of the corner vortex in its spanwise domain is limited by the gap flow through the front- and aft-blade is now confirmed by the wake flow measurements.

Figures 9 b-d) show the corresponding area plots for the total pressure loss distribution 0.5c behind the TE. The corner vortices are quite remarkable in terms of its dimension and absolute values. The $LS_{DF} = 0.5$ tandem configuration shows slightly higher values as the $LS_{DH} = 0.5$ case. This is interesting as the oil flow visualizations of the aft-blades in general show a more calm flow distribution for the $LS_{DF} = 0.5$ tandem blades. However, for the front-blades it is a different scenario and it seems as if the accumulated losses on the front-blade cannot be absorbed by the aft-blades and are more or less transported further.

In absolute values, both tandem configurations reduce the amounted total pressure loss. $\omega_{single} = 0.0901 > \omega_{LS_DF_{0.5}} = 0.0805 > \omega_{LS_DH_{0.5}} = 0.0798$.

CONCLUSIONS

This paper presents an experimental study about the secondary flow development around tandem vanes and in particular the influence of the percent pitch (PP) variation on the secondary flow structure. For this purpose multi-colored oil flow visualizations together with wake flow measurements were conducted. The objective was to get a thorough understanding of the influence of the gap flow on the development of the secondary flows and its influence on the associated losses.

Tandem configurations have the ability to reduce the total pressure losses by limiting the extreme secondary flow development. This study has shown that the two analyzed tandem configurations with different blade loading definitions were capable of reducing the losses especially in the midspan area and repressing the corner vortex expansion. Although the losses in the sidewall area increased in absolute terms, the overall absolute total pressure loss values could be reduced. Interestingly to note

however is that the higher front-blade loading of the $LS_{DF} = 0.5$ tandem blades compared to the $LS_{DH} = 0.5$ blades is reflected in the higher absolute total pressure loss values. This is in accordance with former findings in literature, i.e. Frey and Böhle (2013).

It has also been shown, that the variation of the tangential displacement (Percent Pitch) has a strong influence on the secondary flow phenomena. Especially the development of the corner vortices on the aft-blades is highly affected by the gap size between the front- and the aft-blades. However, the oil-flow visualization only prove this for the aft-blade. The flow around the forward-blade is hardly affected by the position of the aft-blade which was altered by the percent pitch variation. For the flow propagation of the aft-blade one can conclude that if the gap size is reduced to a minimum, 3D separation occurs which cannot be suppressed by the energetic gap flow. This was a little unexpected and needs to be monitored in the future as the single blade does not show any sign of this separation. Nevertheless if the gap size is increased, the flow structures on each of the tandem blades become similar to that of a single vane and the stabilizing influence of the gap flow is lost (cf. Fig 7).

At the moment, the results are in accordance with the available open literature and prove the decision of the authors to more closely examine a percent pitch variation around 90%. More detailed investigations with further variation of the blade loading including Mach number and incidence variations for the same percent pitch settings are planned for the future. Together with accompanying numerical investigations they will further enhance the knowledge, especially in the 3D domain about the influence of the blade loading on the developing flow structures and the associated losses for designing tandem blade configurations.

ACKNOWLEDGEMENTS

The work presented here has been carried out within the framework of the program to support research and development in small and medium-sized enterprises (SMEs) of the Federal Ministry for Econmic Affairs and Energy (BMWi) through the German Federation of Industrial Research Associations (Arbeitsgemeinschaft industrieller Forschungsvereinigungen (AiF) e.V.). It is the scientific result of a research project outlined by the Research Association for Combustion Engines e.V. (Forschungsvereinigung Verbrennungskraftmaschinen e.V. (FVV, Frankfurt)) and conducted by the Institute of Aeronautics and Astronautics (ILR) and the Institute of Fluid Dynamics and Technical Acoustics (ISTA) of the Technische Universität Berlin. The work is funded by the Federal Ministry for Econmic Affairs and Energy (BMWi). Furthermore the author would like to thank the entire project advisory board for their valuable input.

REFERENCES

Falla, G. A. C. (2004). Numerical Investigation of the Flow in Tandem Compressor Cascades. Master's thesis, Institute of Thermal Powerplants Vienna University of Technology.

Frey, T. and Böhle, M. (2013). Flow structure of tandem cascades in the region of the sidewalls. Proceedings of the ASME 2013 Fluids Engineering Division Summer Meeting, 1B(FEDSM2013-16034).

Heinrich, A., Tiedemann, C., and Peitsch, D. (2014). A new linear high speed compressor stator cascade for tandem configurations. In 15th International Symposium on Transport Phenomena and Dynamics of Rotating Machinery, ISROMAC-15, Honolulu, Hawaii, USA.

Liesner, K. and Meyer, R. (2008). Experimental Setup for detailed secondary flow investigation by two-dimensional measurement of Total Pressure Loss coefficients in Compressor Cascades. In

Proc. XIX Biannual symposium on measuring techniques in turbo machinery, number 2008, Sint Genesius Rode, Belgium. von Karman Institute for Fluid Dynamics.

Maltby, R. L. (1962). Flow visualization in wind tunnels using indicators.

McGlumphy, J., Ng, W.-F., Wellborn, S. R., and Kempf, S. (2009). Numerical investigation of tandem airfoils for subsonic axial-flow compressor blades. J. Turbomach., 131.

McGlumphy, J., J. and NG, W.-F. (2007). Overview of a simple design rule for subsonic tandem-airfoil axial-flow Compressor Blades in 2-D. In Proceedings of Student Research Conference, volume 9, page 8, Williamsburg, Virginia. Virginia Space Grant Consortium.

McGlumphy, J. M. (2008). Numerical Investigation of Subsonic Axial-Flow Tandem Airfoils for a Core Compressor Rotor. Dissertation, Virginia Polytechnic Institute and State University.

Schluer, C., Böhle, M., and Cagna, M. (2009). Numerical Investigation of the Secondary Flows and Losses in a High-Turning Tandem Compressor Cascade. In Proceedings of ETC, pages 1–10, Graz.

Sturm, W. (1988). Theoretische und experimentelle Untersuchungen zum Einsatz der Ausblasung als Mittel zur aktiven Beeinflussung der Profilgrenzschicht in hochbelasteten Verzögerungsgittern. PhD thesis, Universität der Bundeswehr München.

Tiedemann, C., Heinrich, A., and Peitsch, D. (2012a). A New Linear High Speed Compressor Stator Cascade for Active Flow Control Investigations. In 6th AIAA Flow Control Conference, number AIAA 2012-3251, New Orleans. American Institute of Aeronautics and Astronautics, American Institute of Aeronautics and Astronautics.

Tiedemann, C., Peitsch, D., Steinberg, S., and King, R. (2012b). Identifikation einer Regelgrösse zur aktiven Strömungskontrolle an einer linearen Verdichterkaskade im kompressiblen Machzahlbereich. In Deutscher Luft-und Raumfahrtkongress 2012, Berlin.

Trehan, S. and Roy, B. (2007). Gap Optimization for Tandem Blades in Axial Flow Compressor/Fan using Computational Tools. In 43rd AIAA/ASME/SAE/ASEE Joint Propulsion Conference & Exhibit, number July, pages 1–11, Cincinnati, Ohio, USA. American Institute of Aeronautics and Astronautics.

Trehan, S., Sodhi, J. S., and Roy, B. (2008). Cascade Studies of Tandem Blades for Axial Flow Compressors/Fans. 44th AIAA/ASME/SAE/ASEE Joint Propulsion Conference & Exhibit.